Available online at www.sciencedirect.com

ScienceDirect

IFAC Papers Online CONFERENCE PAPER ARCHIVE

IFAC PapersOnLine 51-1 (2018) 190–195

Analysis of Handling Performance of Hybrid Electric Vehicles

Kesavan Valis Subramaniyam. C S Nanda Kumar. Shankar C. Subramanian
Department of Engineering Design, IIT Madras, Chennai 600036,
India (Tel: +91-44-22574705; e-mail: shankarram@iitm.ac.in).

Abstract: With increasing focus on addressing fossil fuel shortage and harmful automotive emissions, there has been a growing interest in hybrid electric and pure electric vehicles. A hybrid electric vehicle is driven by a combination of an internal combustion engine and an electric motor. The changes in the powertrain components result in changes in vehicle mass and mass distribution that affects the location of the vehicle's centre of gravity amongst other things. Hence, a hybrid vehicle may not possess the same handling performance as a conventional internal combustion engine driven vehicle. This research work focuses on comparing the handling performance of a conventional engine driven vehicle and a hybrid electric vehicle. The bicycle dynamic model has been used to characterize the cornering dynamics of these two vehicles and the Mimuro plot has been used to analyze their handling characteristics. A sensitivity analysis has been carried out with respect to centre of gravity location and the cornering stiffness of the tires. An approach has been proposed to obtain comparable cornering characteristics in the hybrid vehicle as compared to the engine driven vehicle.

Keywords: internal combustion engine vehicles, hybrid vehicles, under steer coefficient, sensitivity analysis, Mimuro plot, handling performance.

1. INTRODUCTION

Hybrid electric vehicles (HEVs) utilize less fuel and produce lower tailpipe emissions to the environment compared to internal combustion engine (ICE) driven vehicles. The sizing of the motor and the engine along with the distribution of drive energy from them can be optimized to obtain the best possible fuel economy. Further, the presence of regenerative braking allows a part of the vehicle's kinetic energy to be recovered and stored as electrical energy in batteries. While the longitudinal performance of the vehicle and fuel economy are certainly improved by this process, sufficient care must be taken to ensure that the lateral/handling performance of the HEV does not deteriorate.

The cornering characteristics of road vehicles have been studied by various authors. Heydinger et al. (1993) presented the vehicle handling performance comparison analytically and experimentally in frequency domain by considering different steering input signals like triangle pulse, right angle triangle pulse, rectangular pulse, sinusoidal pulse and sinusoidal sweep. Yaw rate, lateral acceleration and roll angle were used to evaluate the vehicle handling performance. Mimuro et al. (1990) formed a rhombus by considering four different parameters related to lateral dynamics and analyzed vehicle handling performance. They considered 20 different vehicles and compared vehicle handling performances for different longitudinal speeds and different tires by considering a triangle pulse steering input.

Kim (2008) analyzed the effect of time constant of lateral force development on vehicle handling performances. He developed a first order transfer function that relates the output lateral force and the input steady state slip angle. The time constant of the transfer function depends on the cornering stiffness of the tire, vehicle longitudinal speed, and an effective spring that was considered as connecting the contact patch and the wheel. Vehicle handling performance was discussed by varying the inflation pressures of the tires. Xia and Willis (1995) analyzed the effect of cornering stiffness of tire on vehicle handling performances and concluded that the high value of cornering stiffness tends to better linear handling performance of a vehicle. Random steer, sinusoidal swept steer, and pulse steer inputs and different tires with distinct cornering stiffness values were considered in their study.

Most studies dealt with the cornering performance of conventional engine driven vehicles. Changes in mass and mass distribution in electric vehicles (EVs) and HEVs would affect the vehicle cornering performance and its analysis using the Mimuro plot forms the objective of this paper. The handling performance of the conventional vehicle and the HEV were first compared by considering the same longitudinal speed and same cornering stiffness values. Then, a method for identifying the changes in mass distribution and cornering stiffness values has been proposed to improve the cornering characteristics of the HEV.

The bicycle model used for analysis is discussed in section 2. In section 3, the Mimuro plots of the conventional base vehicle and the HEV are analyzed. The impact of centre of gravity (CG) location on handling characteristics and the changes to be made to obtain the same handling performance as that of the base vehicle are discussed in section 4. Concluding remarks are discussed in section 5.

2. VEHICLE MODEL

A four-wheeled vehicle is represented as a two-wheeled model or bicycle model where the two (right and left) front wheels are combined as one wheel and the two rear wheels are combined as one wheel. This model is mainly used to analyze the lateral dynamics in the "linear region" of the tire's lateral force vs slip angle response (small slip angles).

10.1016/j.ifacol.2018.05.036

Roll and pitch motions are not considered in this model (Gillespie, 1992).

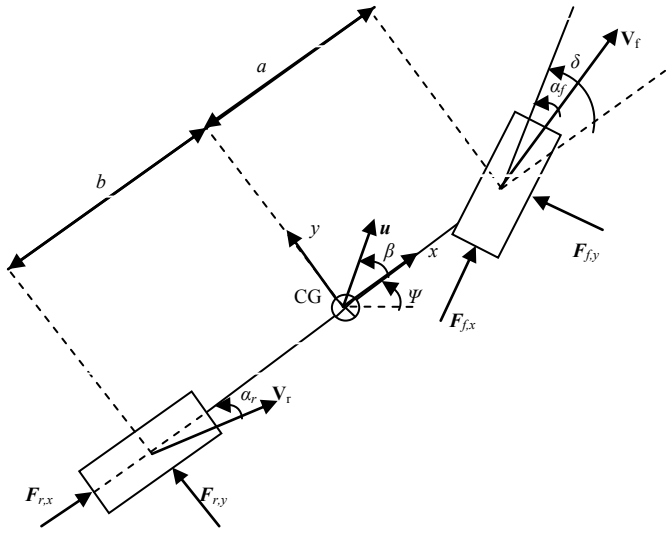

Fig. 1. Vehicle bicycle model

In Fig.1, δ is the steering angle, α_F and α_R are the front and rear slip angle respectively, β is the vehicle slip angle, Ψ is the vehicle yaw angle (at the Centre of Gravity (CG) of the vehicle), $F_{f,x}$ and $F_{r,x}$ are the front and rear longitudinal tire forces respectively, $F_{f,y}$ and $F_{r,y}$ are the front and rear lateral tire forces respectively, **u** is the vehicle velocity (at the CG of the vehicle), $\mathbf{v}_f$ and $\mathbf{v}_r$ are the velocity at the front tire and rear tire respectively, $\dot{x}$ and $\dot{y}$ is the velocity of vehicle along the longitudinal axis and lateral axis respectively, a and b is the distance from CG to front and rear wheel centres respectively.

2.1 Dynamic equations of motion

The governing equations for the bicycle model are

$$F_x(t) = F_{f,x}(t) + F_{r,x}(t) = m\left(\ddot{x}(t) - \dot{\Psi}(t)\dot{y}(t)\right), \quad (1)$$

$$F_y(t) = F_{f,y}(t) + F_{r,y}(t) = m\left(\ddot{y}(t) + \dot{\Psi}(t)\dot{x}(t)\right), \quad (2)$$

$$M_z = I_z\ddot{\Psi}(t) = aF_{f,y}(t) - bF_{r,y}(t), \quad (3)$$

where m is total vehicle mass, F_x is the total longitudinal tire force, F_y is the total lateral tire force, M_z is the rotational moment of vehicle and I_z is the moment of inertia. The bicycle model is a two degree of freedom model, where yaw rate $\left(\dot{\Psi}(t)\right)$ and lateral speed $(\dot{y}(t))$ are the state variables. The model is considered to be front wheel steering where the steering angle is the input.

The state space representation of bicycle model is

$$\begin{bmatrix}\dot{v}(t)\\ \dot{\Psi}(t)\end{bmatrix} = \begin{bmatrix}\frac{-C_f - C_r}{mu} & \frac{-aC_f + bC_r}{mu(t)} - u(t)\\ \frac{-aC_f - bC_r}{I_z u(t)} & \frac{-a^2C_f - b^2C_r}{I_z u(t)}\end{bmatrix}\begin{bmatrix}v(t)\\ \Psi(t)\end{bmatrix} + \begin{bmatrix}\frac{C_f}{m}\\ \frac{aC_f}{I_z}\end{bmatrix}\delta(t), \quad (4)$$

where C_f and C_r are the cornering stiffness of the front and rear tires respectively, I_z is the yaw moment of inertia, and $\dot{\Psi}(t)$ is the yaw rate. The transfer functions relating the yaw rate and the lateral acceleration $(a_y(t))$ to the steering angle input $(\delta(t))$ are

$$\frac{s\Psi(s)}{\delta(s)} = \frac{\frac{aC_f}{I_z}s + \frac{lC_fC_r}{mI_zu}}{s^2 + 2\zeta\omega_n + \omega_n^2}, \quad (5)$$

$$\frac{a_y(s)}{\delta(s)} = \frac{\frac{aC_f}{I_z}s^2 + \frac{lC_fC_r}{mI_zu}s + \frac{lC_fC_r}{mI_z}}{s^2 + 2\zeta\omega_n + \omega_n^2}, \quad (6)$$

where l is the wheel base of the vehicle, which is calculated as, $l = a + b$.

2.2 Transient and steady state analysis

The Mimuro plot illustrates transient and steady state parameters of lateral vehicle dynamics that are derived from (5) and (6). The important parameters used to analyze the transient response are damping ratio (ζ) and natural frequency (f_n) of the system. The mathematical equations for these parameters are given below:

$$\zeta = \frac{1}{2\sqrt{mI_z}}\left[\frac{I_z(C_f + C_r) + m(a^2C_f + b^2C_r)}{l\sqrt{C_fC_r}\sqrt{1 + k_1u^2}}\right], \quad (7)$$

$$f_n = \frac{l}{2\pi u}\sqrt{\frac{C_fC_r(1 + k_1u^2)}{mI_z}}, \quad (8)$$

$$k_1 = \frac{m}{l^2}\left[\frac{b}{C_f} - \frac{a}{C_r}\right]. \quad (9)$$

The yaw rate steady state gain (a_1) and phase delay of lateral acceleration response at 1 Hz are considered to analyze the steady state handling characteristic of the vehicle, which are respectively given by

$$a_1 = \frac{u}{l(1 + k_1u^2)}, \quad (10)$$

$$\phi = \tan^{-1}\left(\frac{2\pi C_r lb}{u(lC_r - 4\pi^2I_z)}\right) - \tan^{-1}\left(\frac{2\zeta f_n}{f_n^2 - 1}\right). \quad (11)$$

2.3 Vehicle stability

To evaluate the vehicle stability, under steer coefficient was considered and it is given by

$$k = \frac{w_f}{C_f} - \frac{w_r}{C_r}, \quad (12)$$

where w_f is the front axle load and w_r is the rear axle load of the vehicle. The vehicle handling performance depends on the value of k. The vehicle which has a positive k value is called an under steer vehicle, if the value of k is exactly zero then that vehicle is called a neutral steer vehicle and if the value of k is negative then the vehicle is called an over steer vehicle.

For an over steered vehicle, the value of k is negative and the critical longitudinal speed at which the vehicle becomes unstable is given by

$$u_{cr} = \sqrt{\frac{gl}{-k}}, \tag{13}$$

where g is the acceleration due to gravity.

2.4 Conventional and Hybrid Electric vehicle parameters

Mahindra Maxximo plus vehicle (Mahindra Maxximo Plus. Technical specification, 2014) was considered as the base vehicle (conventional) in this study. The same vehicle was converted as a series hybrid electric vehicle (SHEV) by Kumar and Subramanian to study about the combined braking performance that includes the regenerative braking and friction braking. These two sets of vehicle parameters were considered to study about the handling performance between the conventional and hybrid vehicles. The CG location of both vehicles was measured with the maximum allowable load. The value of I_z was calculated by considering the vehicle front axle mass (m_f) and rear axle mass (m_r) as two point masses, which are connected by a mass-less rod and it is given by

$$I_z = m_f a^2 + m_r b^2. \tag{14}$$

Another important parameter is the tire cornering stiffness and it was calculated from the initial slope of side force (F_y) vs side slip angle (α) plot, which is shown in Fig. 2, and is given by

$$C = \frac{\Delta F_y}{\Delta \alpha}. \tag{15}$$

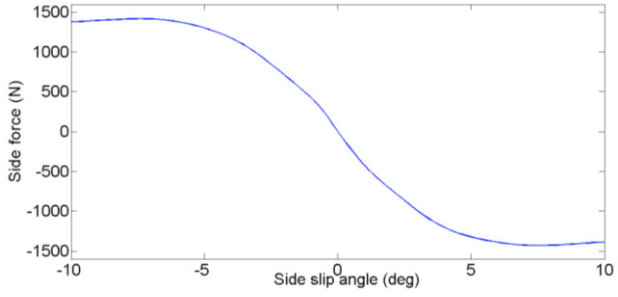

Fig. 2. Side force Vs Side slip angle

Figure 2 was generated from IPG CarMaker® by considering the nearest tire that is used in the vehicle under study. Since the same tire was used in all four wheels, the cornering stiffness value was the same for both front and rear tires.

Table 1. Vehicle parameters

Parameter	Value	
	Conventional vehicle	HEV
m	1800 kg	1800 kg
a	0.9 m	1.23 m
b	0.94 m	0.61 m
I_z	1522 kg m^2	2042 kg m^2
C_f=C_r	52626 N/rad	52626 N/rad (in case of same tire)

To corroborate the bicycle dynamic model, the yaw rate and the lateral acceleration response of the conventional vehicle from CarMaker® was compared with the bicycle model by considering the steering wheel input as per ISO13674 (International standard 13674, 2003) standard and the results are shown in Fig. 3. Given the good agreement between the two, the bicycle model is a reasonable mode to analyze the handling characteristics of the vehicle under study. Table 1 shows the conventional vehicle and SHEV parameter values. It could be observed that the vehicle CG has shifted to the rear in the HEV.

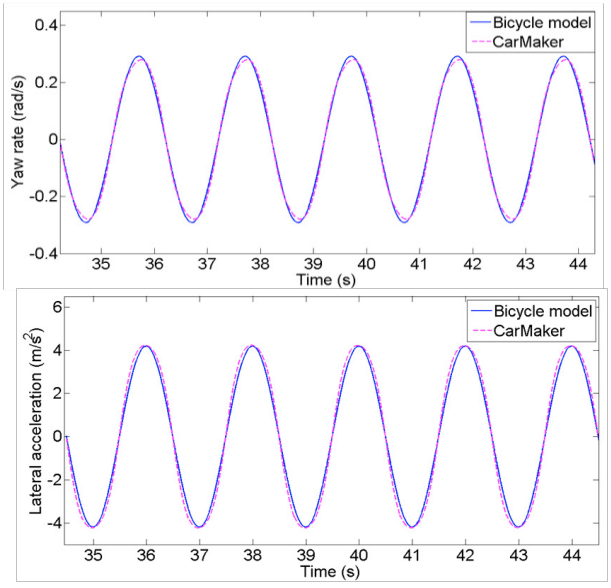

Fig. 3. Comparison of CarMaker® and Bicycle model

3. MIMURO PLOT

Mimuro plot was used to evaluate the handling performance of the vehicles. It uses four different parameters that are extracted from the vehicle lateral dynamic motion of equations (from vehicle bicycle model). The four parameters are:

i. Steady state yaw rate gain (a_1)

ii. Natural frequency of yaw rate response (f_n)

iii. Damping ratio of yaw rate response (ζ)

iv. Phase delay of lateral acceleration response at 1 Hz (ϕ)

These four parameters are plotted on four different axes to form a rhombus whose area is correlated with overall vehicle handling quality. Figure 4 shows a typical interpretation of the Mimuro plot. If the rhombus moves upward and to the right (single dotted line direction on the Fig. 4), then the vehicle is said to be more under steered. If the rhombus moves downward and to the left (double dotted line direction on the Fig. 4), then the vehicle is said to be more over steered.

The evolution of these four parameters is closely related with driver's subjective interpretation of lateral vehicle response. The steady state yaw rate gain is related with heading

easiness; natural frequency of yaw velocity is related with heading responsiveness, damping ratio of yaw velocity is related with directional damping and phase delay at 1 Hz of lateral acceleration related with following controllability (Mimuro et al., 1990).

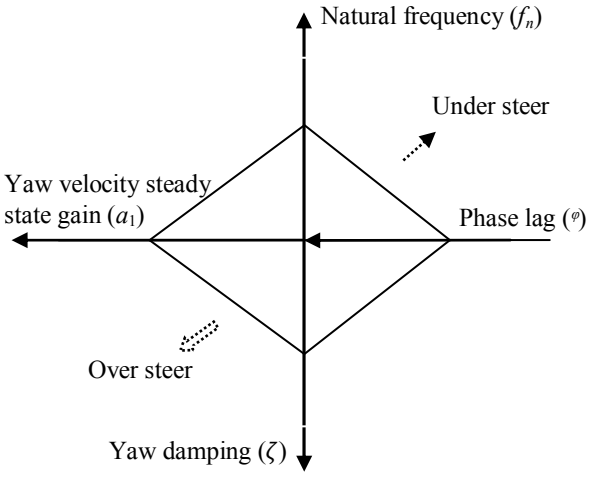

Fig. 4. Mimuro plot

3.1 Base vehicle Mimuro plot

For the base vehicle parameters, under steer coefficient was calculated using (12) and it gives a positive value. Hence, the vehicle is under steered and its cornering response is stable. By considering different longitudinal speeds, the Mimuro plots are plotted as shown in Fig. 5. From Fig. 5, it can be observed that as longitudinal speed increases, the vehicle has a tendency to become over steered. As speed of the vehicle increases, natural frequency of yaw rate and damping ratio of yaw rate decrease. These physically signifies a decrease in heading responsiveness and directional damping of the vehicle respectively. The steady state yaw rate gain increases as speed increases, which signifies improvement in the vehicle heading easiness. The phase delay of lateral acceleration at 1 Hz increases as speed increases, which signifies a decrease in the following controllability .

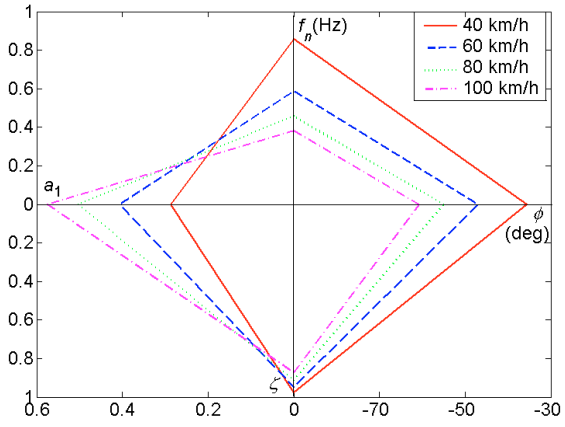

Fig. 5. Base vehicle Mimuro plot

3.2 SHEV Mimuro plot

A HEV is driven by two energy sources namely ICE and electrical motor. HEVs can be divided into different architecture depending on the connection between these two energy sources (Shen et al., 2011). The different architectures are as follows:

- Series: An Internal Combustion (IC) engine is used to charge the battery and an electrical motor alone is used to drive the vehicle.
- Parallel: Both IC engine and electrical motor will drive the vehicle together.
- Series-parallel: It can be operated like series or parallel depending on the requirement.

The base vehicle was converted as SHEV by locating the electric motor and battery near to the rear axle. Now, for the same cornering stiffness value with the new CG location, the under steer coefficient was calculated and it was found to be negative. Hence, the converted SHEV is in over steered condition (Fig. 6) and the corresponding critical speed of the vehicle is 12.6 m/s. Since this is relatively a lower value of critical speed, it is necessary to adjust the cornering stiffness value to get the same cornering performance as the base vehicle.

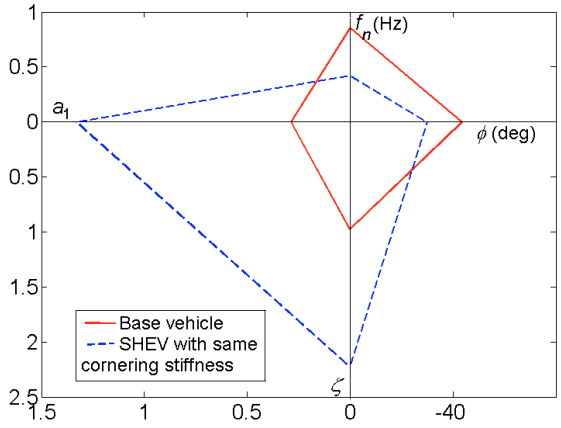

Fig. 6. Base vehicle SHEV Mimuro plot comparison

4. IMPACT OF HYBRID ELECTRIC POWER TRAIN

HEVs additionally use electric motor and batteries as compared to conventional vehicles whose size depends the type of HEV architecture. These additional components change the load distribution between the front and rear axles and the yaw moment of inertia. The changes in these parameter affect the vehicle's lateral dynamics and its stability. It is possible to improve the handling performance and vehicle stability close to that of conventional vehicle by tuning the under steer coefficient that depends on the adjustable parameters (CG location and cornering stiffness). Hence, a corresponding analysis has been carried out.

4.1 Adjusting cornering stiffness for a fixed CG location

To analyze the under steer coefficient variation with respect to CG location, CG location from the front axle was varied from 0.4 m to 1.4 m in steps of 0.02 m and the under steer

coefficient was calculated. Figure 7 shows the variation of under steer coefficient value with respect to a. When the CG location from the front axle is increased, the under steer coefficient value decreases linearly. The sign of under steer coefficient changes at a particular position of CG location and the corresponding critical speed of the vehicle is 49.74 m/s. Figure 8 shows that the critical speed decreases exponentially as the CG location is moved further closer to the rear axle from this position.

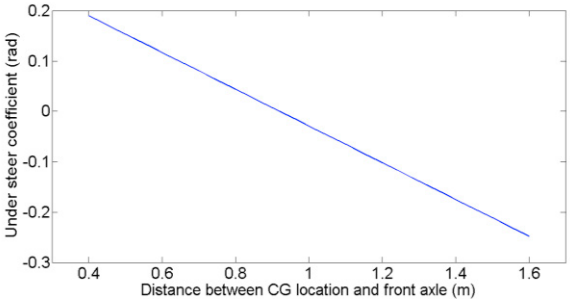

Fig. 7. Under steer coefficient vs CG location from front axle (a)

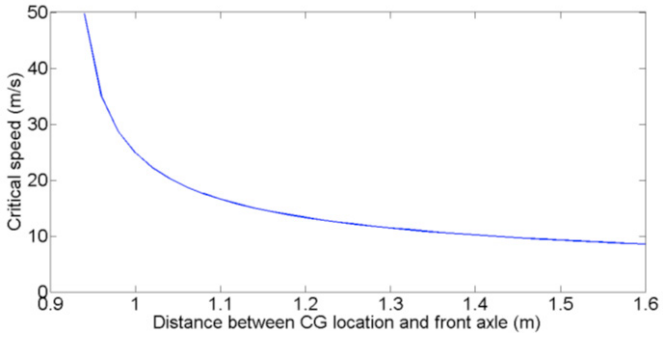

Fig. 8. Critical speed with respect to distance from CG location to front axle (a)

The Mimuro plot of a base vehicle, with different values of a (increasing order) is shown in Fig. 9 and it was observed that the vehicle is becoming more over steered when the CG location is moving towards rear axle of the vehicle.

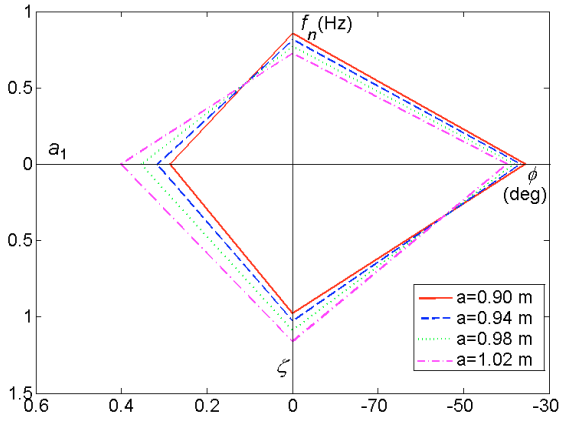

Fig. 9. Mimuro plot for increasing value of a

Considering a_1 and b_1 as the distance from CG to front and rear axle of the hybrid vehicle respectively, the cornering stiffness values that can yield the same understeer coefficient as that of the base vehicle can be calculated as

$$C_{f1} = \frac{b_1}{\left[\frac{a_1}{C_r} + \frac{kl}{w}\right]}, \tag{16}$$

$$C_{r1} = \frac{a_1}{\left[\frac{b_1}{C_f} - \frac{kl}{w}\right]}. \tag{17}$$

Equation (16) provides the new front tire cornering stiffness value by keeping the same rear tire cornering stiffness for a new CG location and (17) provides the new rear tire cornering stiffness value by keeping the same front tire cornering stiffness for a new CG location.

4.2 Adjusting both CG location and cornering stiffness

There is a possibility of changing both CG location and the cornering stiffness to achieve same base vehicle characteristics such that the ratio of $\frac{b}{C_f}$ and/or the ratio of $\frac{a}{C_r}$ are controlled. Equation (12) can be written as

$$k = \frac{w}{l}\left[\frac{b}{C_f} - \frac{a}{C_r}\right], \tag{18}$$

$$k = \frac{w}{l}[r_1 - r_2], \tag{19}$$

where $r_1 = \frac{b}{C_f}$ and $r_2 = \frac{a}{C_r}$.

Let the percentage of movement of CG location with respect to wheelbase be x. Then, the new CG location is given by

$$a_1 = a \pm x_1, \tag{20}$$

and

$$b_1 = b \pm x_1, \tag{21}$$

where $x_1 = l\frac{x}{100}$. The new under steer coefficient is given by

$$k_{new} = \frac{w}{l}\left[\frac{b_1}{C_{f,new}} - \frac{a_1}{C_{r,new}}\right], \tag{22}$$

$$k_{new} = \frac{w}{l}[r_{1,new} - r_{2,new}], \tag{23}$$

where $r_{1,new} = \frac{b_1}{C_{f,new}}$ and $r_{2,new} = \frac{a_1}{C_{r,new}}$. To get the same value of under steer coefficient, one possible way is to maintain the same values of $r_{1,new}$ and $r_{2,new}$ as that of the base vehicle.

This yields

$$C_{f,new} = \left(\frac{b_1}{b}\right)C_f, \tag{24}$$

and

$$C_{r,new} = \left(\frac{a_1}{a}\right)C_r. \tag{25}$$

By considering the SHEV's CG location and u=11.11 m/s (since the critical speed for the corresponding CG location is 12.6 m/s), all the above possible cases are used to calculate the cornering stiffness values and the Mimuro plot was drawn

with corresponding values of cornering stiffness as shown in Fig. 10.

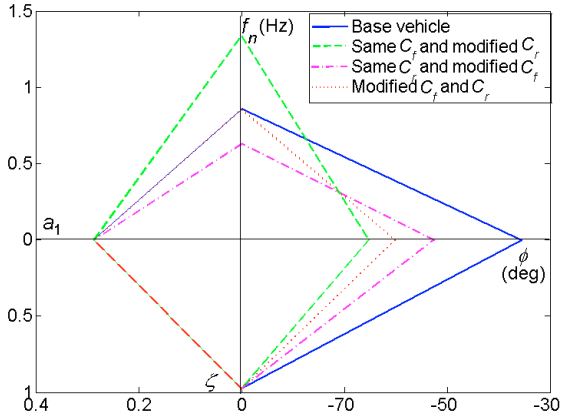

Fig. 10. Comparison of Mimuro plot for a=1.23 m

From Fig. 10, it was observed that while changing any one of the cornering stiffness values, yaw rate steady state gain and yaw rate damping ratio match with that of the base vehicle. While modifying both the cornering stiffness values using the proposed method, natural frequency of yaw rate also matches in addition to the two parameters. This means that the heading easiness, heading responsiveness, and directional damping of the HEV would be the same as that of the conventional vehicle. But, there is deterioration in the following controllability of the HEV. The Mimuro plot parameter values and the corresponding percentage change are shown in Table 2 and Table 3 respectively.

Table 2. Comparison of Mimuro plot parameter

Mimuro parameter	Base vehicle	SHEV (with same C_f and same C_r)	Same C_f and new C_r	Same C_r and new C_f	New C_f and new C_r
a_1	0.2876	1.3308	0.2876	0.2876	0.2876
ζ	0.9762	2.2299	0.9765	0.9761	0.9762
f_n (Hz)	0.8585	0.4238	1.3391	0.6318	0.8585
ϕ (deg)	-35.52	-52.5140	-65.1811	-52.5140	-60.0113

Table 3. Comparison of percentage change.

Mimuro parameter	Same C_f and new C_r	Same C_r and new C_f	New C_f and new C_r
a_1	0	0	0
ζ	-0.0373	0.0102	0
f_n (Hz)	-55.9813	28.5032	0
ϕ (deg)	-83.5053	-32.3571	-68.9507

From Table 3, it can be observed that the changing both the cornering stiffness values using the proposed method brings the HEV performance closer to the conventional vehicle.

5. CONCLUSIONS

This study evaluated the cornering performance of a conventional engine driven vehicle and the corresponding HEV using the bicycle model and the Mimuro plot. It was observed that as the speed of the conventional vehicle increases, the vehicle tends to be more over steer. It was observed that the designed HEV was in oversteer. Hence, a method was proposed to adjust the tire cornering stiffnesses to match the cornering performance of the HEV with that of the conventional vehicle. It was observed that changing both the cornering stiffness values gave better results compared to changing them separately.

REFERENCES

Gillespie, T.D., (1992). *Fundamentals of vehicle dynamics*, Society of Automotive Engineers, Warrendale, PA.

Heydinger, G., Grygier, P., and Lee, S., (1993). Pulse Testing Techniques Applied to Vehicle Handling Dynamics, *International Congress and Exposition*, USA, Detroit, Michigan: SAE.

Kim, J., (2008). Analysis of Handling Performance Based on Simplified Lateral Vehicle Dynamics, *International Journal of Automotive Technology*, 9 (6), p. 687−693.

Kumar, CS.N., and Subramanian, S.C., (2016). Cooperative Control of Regenerative Braking and Friction Braking for a Hybrid Electric Vehicle, *Proc IMechE Part D: J Automobile Engineering*,230 (1), p.103-116.

Mimuro, T., Ohsaki, M., Yasunaga, H., and Satoh, K., (1990). Four Parameter Evaluation Method of Lateral Transient Response, *Passenger Car Congress and Exposition*, USA, Dearborn, Michigan: SAE.

Mahindra Maxximo Plus, Technical specification, (2014). URL: www.mahindramaxximoplus.com/

Road vehicles - Test methods part 1., (2003). *International standard 13674* (wave test).

Shen, C., Shan, P., and Gao, T., (2011). A comprehensive overview of hybrid electric vehicles, *Int. J. Veh. Technol.*, 2011, p.1305-1313.

Xia, X., and Willis, J., (1995). The Effects of Tire Cornering Stiffness on Vehicle Linear Handling Performance, *International Congress and Exposition*, USA, Detroit, Michigan: SAE.